

Calculation of turbulence flow field around photovoltaic inclined plate based on CFD

Shui-Sheng Xu^{1,*}, Ji-Wei Shen²

1 TONKING NEW ENERGY TECHNOLOGY (JIANGSHAN) CO., LTD., Quzhou, 324100, China;

2 College of Mechanical Engineering, Quzhou University, Quzhou, 324000, China;

Abstract: In order to investigate the effects of inclination angle and wind velocity on the flow characteristics of the outer domain of photovoltaic inclined plate, four models of photovoltaic inclined plate with different inclination angles are created in this paper. Based on the computational fluid dynamics method, the numerical wind tunnel simulation of photovoltaic inclined plate is established, which mainly simulates the photovoltaic inclined plate in the working condition with the inclination angle θ from 15 to 60° and the wind velocity v from 5 to 20m/s, and then the wind velocity and streamline distribution on the outer domain of the photovoltaic inclined plate are obtained and the drag coefficients of photovoltaic inclined plates with different inclinations are analyzed comparatively. The results show that as the inclination angle of the inclined plate increases, the area of the cavity zone formed at the back of the inclined plate is larger, the intensity of the vortex is larger, and the drag coefficient of the inclined plate is larger. As the inlet wind velocity increases, the intensity of the vortex is greater. However, the region area of cavity zone and vortex zone is almost unaffected by the wind speed.

Keywords: Photovoltaic panel; Numerical analysis; Windborne; Drag coefficient

Date of Submission: 21-09-2023

Date of Acceptance: 05-10-2023

I. Introduction

As technology advances and environmental awareness increases, the global energy landscape is changing. Photovoltaic power generation as renewable energy with zero pollution is a key project for energy development [1]. However, photovoltaic power generation systems are often damaged by natural disasters such as storms and typhoons, resulting in economic losses and casualties. Therefore, wind resistance is a major issue in the photovoltaic power generation system.

At present, there have been many scholars who have studied the windborne and mechanics of photovoltaic inclined plate by numerical simulation or experiment. Miller et al. measured the windborne on the PV panels using manometric system and found that the wind pressure on the surface of the PV panels is uniformly distributed [2]. He et al. proposed a new wind pressure distribution model for photovoltaic arrays combined with wind tunnel experiments, and found that the wind pressure acted on the photovoltaic arrays has an inhomogeneous and trapezoidal distribution [3]. Jiang et al. used numerical simulation to analyze the effects of wind angle, mounting inclination of PV array and longitudinal distance of PV panels on windborne loads on PV arrays and the bending moments. The results show that the extreme values of the body shape coefficient and bending moment coefficient correspond to different wind angles, and the windborne loads do not vary significantly with the longitudinal distance of the PV panels [4]. Gong et al. investigated the windborne loads on roof photovoltaic (PV) modules using a rigid model surface manometry method, and found that the distribution of windborne pressures acting on PV panels has an asymptotic nature; within the range of the test tilt angle, the windborne loads acting on PV panels panels roughly show an upward trend as the inclination angle of the PV panels increases [5]. Hu et al. carried out windborne calculations for a photovoltaic power generation system, obtained the system's stresses under extreme wind force, and proposed an improvement program [6]. ABIOLA et al. analyzed the hydrostatic characteristics of photovoltaic devices under windborne loads and found that the pressure on the photovoltaic mounts increases with increasing height angle [7]. Wei et al. numerically analyzed the mechanical properties of fixed PV mounts and found that reinforcement of the front structure or complete elimination of settlement at the front support should be considered in the design [8]. PFAHLA and XIONG et al. studied the structural stability of photovoltaic (PV) devices and concluded that the pressure at the edges of PV panels is the highest and the bottom of PV mounts is the most susceptible to shear damage under dynamic windborne loads [9,10].

In conclusion, scholars have studied photovoltaic power generation systems in terms of windborne effects and mechanical properties. However, the effects of flow performance in the outer domain of a photovoltaic inclined plate caused by changes in inclination and wind velocity have not been thoroughly and systematically investigated. Based on it, this paper establishes four kinds of photovoltaic inclined plate outer

basin models with different inclination angles and carries out numerical calculations under different wind velocities, expecting to grasp the flow effects caused by changes in inclination angles and wind velocities.

II. Calculation model and method

2.1 Calculation model

The simplified structure of the photovoltaic inclined plate in this paper is shown in Fig. 1 in cm. By changing the inclination angle θ , the models of photovoltaic inclined plates with different inclination angles and the computational models of the outer watershed are obtained. The outer watershed calculation model is shown in Fig. 2. The photovoltaic inclined plate is centered on the support columns throughout the outer watershed calculation domain; the wind direction enters from the front of the photovoltaic inclined plate.

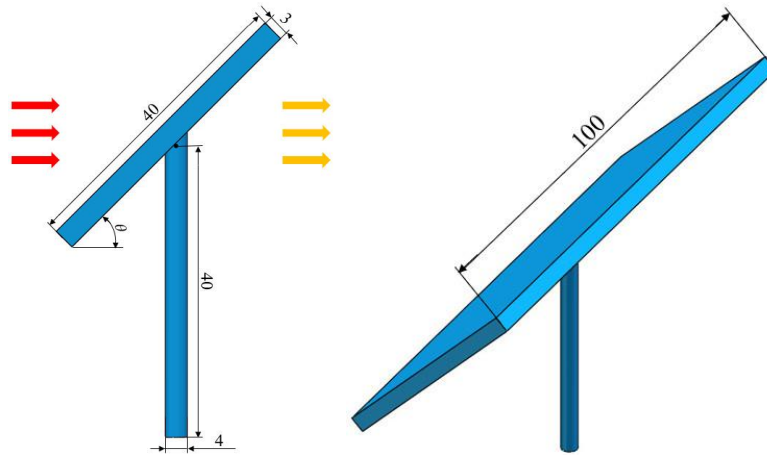


Fig. 1 Simplified model of photovoltaic inclined plate

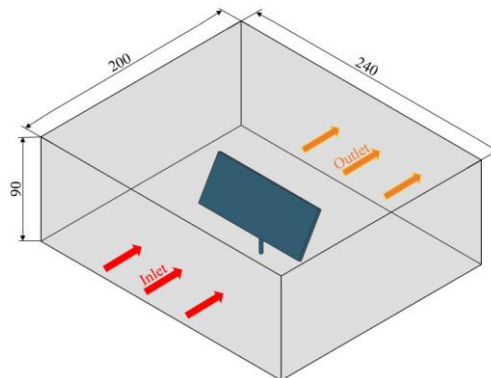
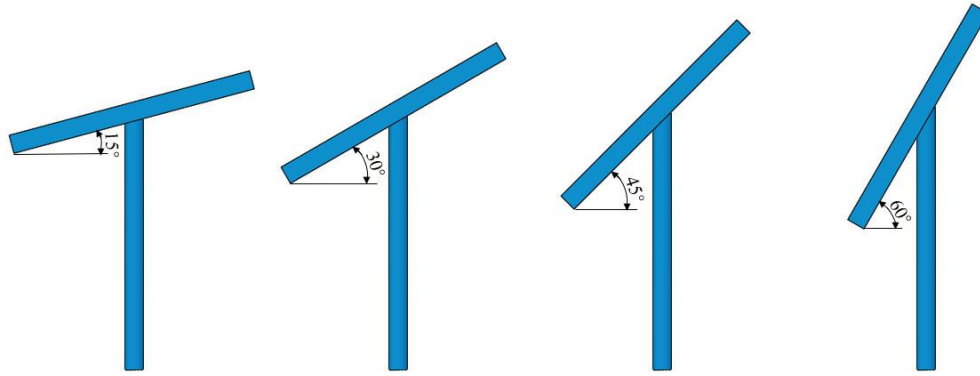


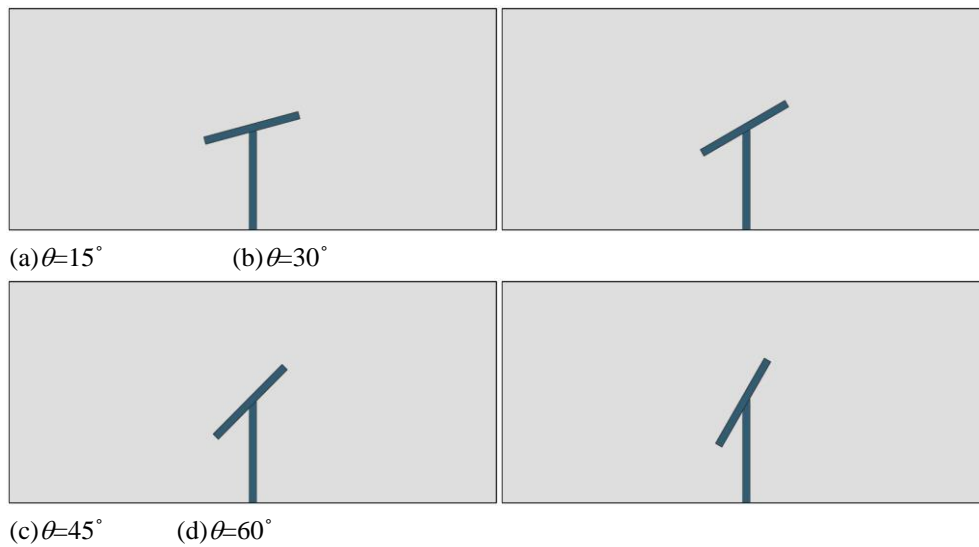
Fig. 2 Calculation model of the outer watershed of photovoltaic inclined plate

Except for the inclination angle θ , all the structural parameters of the four photovoltaic inclined plates in this paper are of the same size. By changing the inclination angle θ , the final photovoltaic inclined plates with different inclination angles are obtained as shown in Fig. 3. And accordingly, four outer watershed models with different inclination angles are obtained, and the calculation watersheds are shown in Fig. 4. In this paper, the numerical simulation of the flow in the outer watershed under the inclination angle θ of 15° , 30° , 45° , 60° and the incoming velocity v of 5m/s, 10m/s, 15m/s and 20m/s is carried out, and finally the characteristics of the velocity distribution, streamline change and so on are obtained under different inclination angles and wind velocities.



(a) $\theta=15^\circ$ (b) $\theta=30^\circ$ (c) $\theta=45^\circ$ (d) $\theta=60^\circ$

Fig. 3 Photovoltaic inclined plates at different inclination angles



(a) $\theta=15^\circ$ (b) $\theta=30^\circ$
(c) $\theta=45^\circ$ (d) $\theta=60^\circ$

Fig. 4 Calculation domain of the outer watershed at different inclination angles

2.2 Calculation method

In this paper, numerical calculations of steady, incompressible, three-dimensional viscous flow in the outer watershed of photovoltaic inclined plate are carried out based on ANSYS-FLUENT software. The control equations to be solved are

$$\frac{\partial}{\partial t}(\rho k) + \frac{\partial}{\partial x_i}(\rho k u_i) = \frac{\partial}{\partial x_j} \left[\left(\mu + \frac{\mu_t}{\sigma_k} \right) \frac{\partial k}{\partial x_j} \right] + G_k + G_b - \rho \varepsilon - Y_M + S_k \quad (1)$$

$$\frac{\partial}{\partial t}(\rho \varepsilon) + \frac{\partial}{\partial x_i}(\rho \varepsilon u_i) = \frac{\partial}{\partial x_j} \left[\left(\mu + \frac{\mu_t}{\sigma_\varepsilon} \right) \frac{\partial \varepsilon}{\partial x_j} \right] + G_{1\varepsilon} \frac{\varepsilon}{k} (G_k + G_{3\varepsilon} G_b) - C_{2\varepsilon} \rho \frac{\varepsilon^2}{k} + S_\varepsilon \quad (2)$$

where: $k = \frac{1}{2}(\overline{u'^2} + \overline{v'^2} + \overline{w'^2})$, $\varepsilon = \frac{\mu}{\rho} \left(\frac{\partial u'_i}{\partial x_k} \frac{\partial u'_i}{\partial x_k} \right)$, $\mu_t = \rho C_\mu \frac{k^2}{\varepsilon}$, C_μ is empirical constant, G_k

is the generating term for k due to the mean gradient of velocity, G_b is the generating term for k caused by buoyancy, Y_M is the contribution term to the pulsation expansion in pressurizable turbulent flows, $C_{1\varepsilon}$, $C_{2\varepsilon}$, $C_{3\varepsilon}$ are empirical constants, σ_k and σ_ε are the Prandtl numbers corresponding to k and ε , S_k , S_ε are wall terms.

Based on ICEM software, the structure of the outer watershed model was divided using a tetrahedral grid. For the four inclination scenarios ($\theta = 15^\circ, 30^\circ, 45^\circ$, and 60°), the corresponding number of calculation grids for the outer watershed model is about 730955, 726816, 725223, and 719427, respectively, which is sufficient. As an example, the grid diagram of the outer watershed at $\theta = 45^\circ$ is shown in Fig. 5. The flow medium in the

calculations is air, which is solved using a three-dimensional double precision solver. Velocity inlet boundary condition is used at the inlet; pressure outlet boundary condition is used at the outlet.

Velocity inlet boundary condition is applicable to incompressible flow problems where the magnitude, direction or each velocity component needs to be specified. Pressure inlet boundary condition is usually used when the fluid pressure at the inlet is known and the flow velocity is unknown, and is applicable for both computationally compressible and incompressible problems, where the size of the total inlet pressure needs to be specified. For incompressible flow, the total pressure, the static pressure, and the velocity of the fluid have the following relationship:

$$p_t = p_s + \frac{1}{2} \rho v^2 \quad (3)$$

At the inlet of the calculation domain of this paper, the velocity inlet boundary condition is chosen. Based on the conservation of mass and the incompressibility of the fluid, the value of the axial velocity at the inlet can be given according to the regulated flow rate and the size of the inlet piping, and assuming that the tangential and radial velocities are zero. The turbulent kinetic energy k and turbulent dissipation rate ε at the inlet can be determined by the following equation:

$$k = \frac{3}{2} (\overline{Iu})^2 \quad (4)$$

$$\varepsilon = C_\mu^{3/4} \frac{k^{3/2}}{l} \quad (5)$$

where $l = 0.07L$, and L is the characteristic length (the value taken in this paper is the diameter at the inlet).

I is the turbulence intensity, $I \approx 0.16 \text{Re}^{-1/8}$, $\text{Re} = \frac{\overline{u} \cdot L}{\nu}$, \overline{u} is the average velocity at the inlet.

$C_\mu \approx 0.09$ is the empirical constant in the turbulence model.

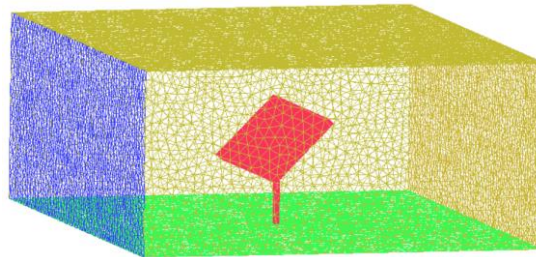


Fig. 5 Outer watershed grid

III. Analysis of results

3.1 Effect of inclination on outflow field

In order to investigate the effect of the inclined angle of the photovoltaic inclined plate on the flow characteristics of the outer flow field, the flow of the outer flow field at each inclined angle was simulated at the wind velocity $v=10\text{m/s}$. At the same time, to better describe the flow characteristics of the outer watershed of the photovoltaic inclined plate, two of the inner cross sections are selected as the analysis object for comparative analysis of velocity distribution, streamline changes and other characteristics. The location of reference surfaces Surface1 and Surface2 in the outer flow field is shown in Fig. 6.

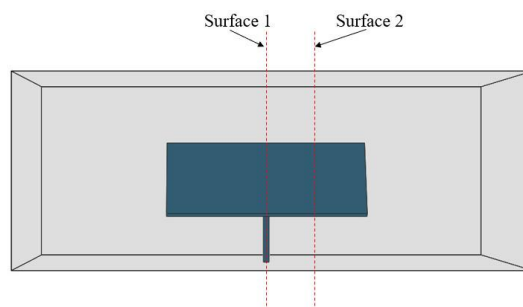


Fig. 6 Reference surface identification

The velocity distribution of Surface1 at different inclination angles is shown in Fig. 7. Overall, the flow field of the photovoltaic inclined plate can be roughly divided into displacement zones before the airflow comes into contact with the photovoltaic inclined plate; separation zones generated when the airflow flows through the photovoltaic inclined plate; and cavity zones formed by the airflow on the backside of the photovoltaic inclined plate. As can be seen in Fig. 7, the air flow through the inclined plate creates a cavity area on the backside of the inclined plate and the support column. As the inclined angle of the photovoltaic inclined plate increases, the cavity area at the back of the inclined plate increases significantly. When the inclined angle is small, the width of the cavity area is narrow; while the inclined angle increases, the width of the cavity area increases significantly. It is also found that as the inclination angle increases, a cavity zone is formed at the lower end of the front face of the photovoltaic inclined plate. At an inclination angle of $\theta = 15^\circ$, only a very small cavity area exists at the lower end of the front face of the inclined plate. Whereas, as the inclination angle increases, a larger cavity area is formed at the lower end of the front face of the inclined plate at the photovoltaic inclined plate inclination angles of $\theta = 45^\circ$ and $\theta = 60^\circ$. Also, the wind velocity in the separation zone increases as the inclination angle increases. The maximum wind velocity in the separation zone is about 15m/s at the condition of inclination $\theta = 15^\circ$, while the maximum wind velocity in the separation zone is about 17.5m/s at the condition of inclination $\theta = 60^\circ$. As can be seen, the wind velocity in the separation zone increases with increasing inclination at the same inlet wind velocity.

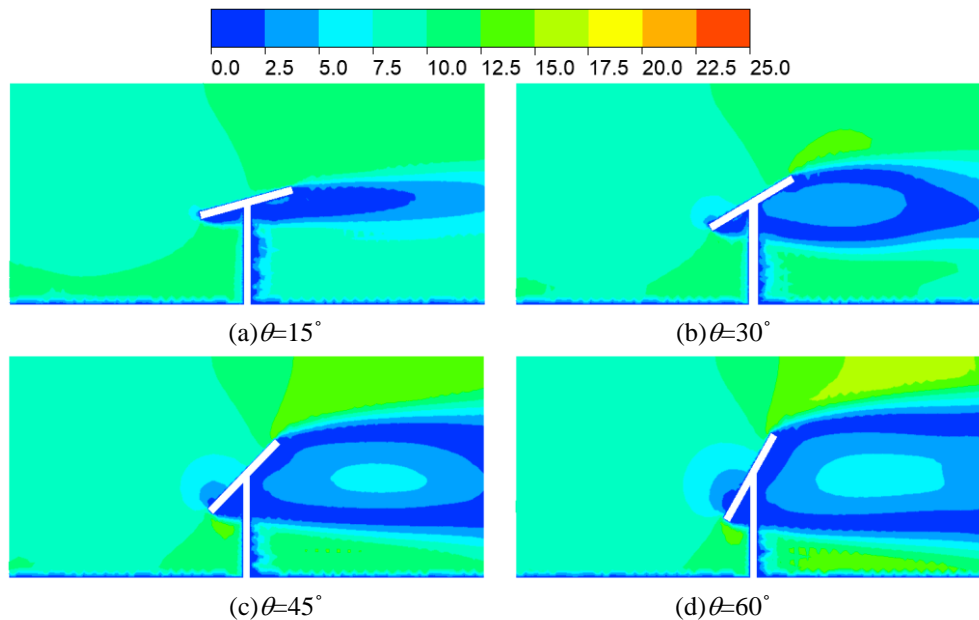


Fig. 7 Velocity distribution of Surface1 at different inclination angles (m/s)

The streamline diagram of Surface1 at different inclination angles is shown in Figure 8. Compared Fig. 8 with Fig. 7, it is found that the vortex region at each inclination angle overlaps extremely with the cavity region described above. At either inclined angle, two vortices are formed on the backside of the photovoltaic inclined plate. As the inclination increases, the two vortices become more distinct. It was also found that the vortex region is larger and the streamlines in the vortex region are denser and the intensity of the vortex is greater under large inclination conditions.

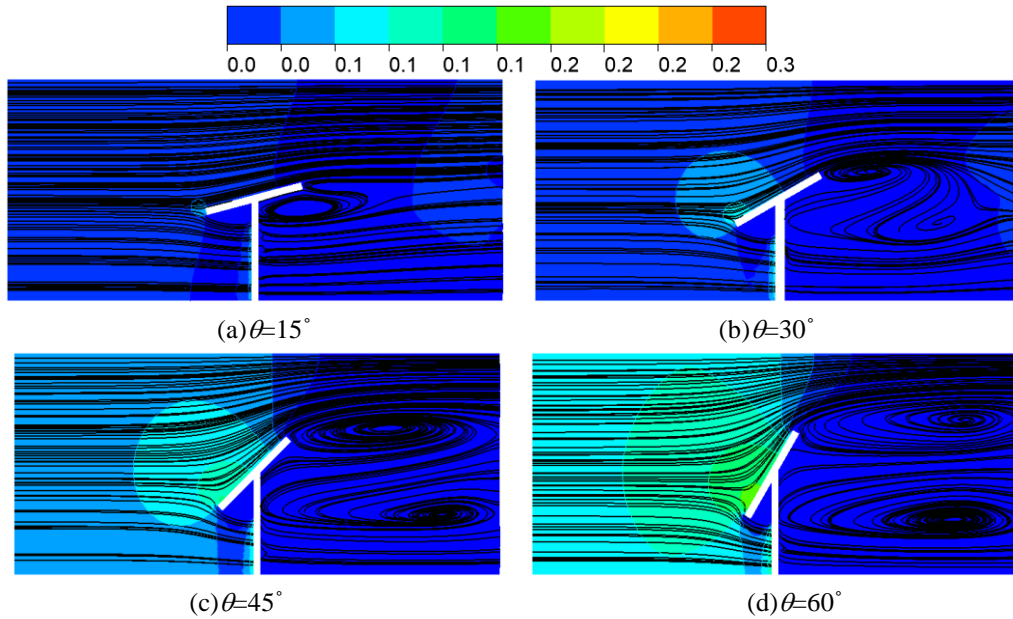


Fig. 8 Streamlines of Surface1 at different inclination angles (kPa)

The streamline diagram of Surface2 at different inclination angles is shown in Figure 7. The support columns are less impactful on the Surface 2 relative to the Surface 1. Compared with Fig. 9 and Fig. 8, there is a change in the area of vortex formation. On Surface 1, due to the blocking effect of the support column, the vortices all appear on the backside of the support column and the upper half of the inclined plate. In contrast, on the Surface 2, the vortex area moves closer to the entire back of the inclined plate, generating vortices close to the back of the inclined plate. It is also found that as the inclination increases, the vortex becomes more distinct and the vortex affects a larger area.

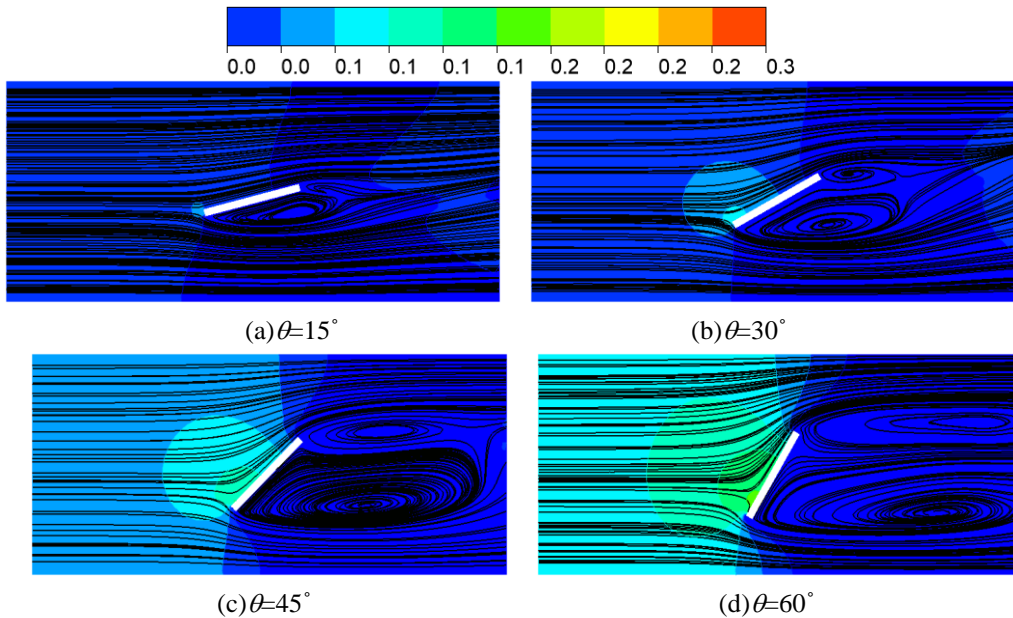


Fig. 9 Streamlines of Surface2 at different inclination angles (kPa)

The air flow through the photovoltaic inclined plate creates resistance, which is caused by the wind pressure. The drag coefficient is the ratio of drag to the dynamic pressure of the airflow and the reference area, and its variation describes the variation of the drag applied to the photovoltaic inclined plate. After CFD calculation and monitoring the drag coefficient, the drag coefficients at different inclination angles are obtained as shown in Fig. 10.

When the photovoltaic inclined plate is at different inclination angle, its wind area is different, and the flow velocity around the photovoltaic inclined plate is different, thus the windborne load on the photovoltaic

inclined plate is different. As clearly seen in Fig. 10, the wind area of the photovoltaic inclined plate increases as the inclination angle increases, and the drag coefficient increases. At inclination angles θ of 15° , 30° , 45° , and 60° , the corresponding drag coefficients are 0.05387, 0.12317, 0.20962, and 0.30698, respectively. As can be easily seen, the wind area is the smallest and the drag coefficient is the smallest when the inclination angle $\theta=15^\circ$, and the wind area is the largest and the drag coefficient is the largest when the inclination angle $\theta=60^\circ$.

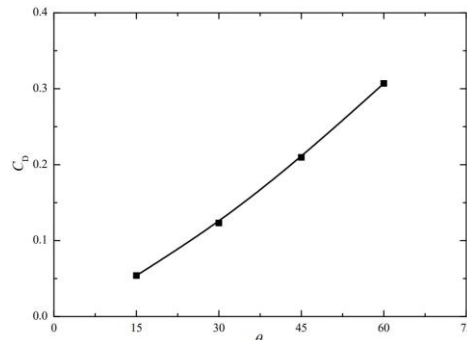


Fig. 10 Drag coefficient at different inclination angles

3.2 Effect of wind velocity on the outflow field

In order to investigate the effect of wind velocity on the flow characteristics of the outer flow field of the photovoltaic inclined plate, the flow of the outer flow field was simulated at different wind velocities at an inclination angle of $\theta=45^\circ$. Meanwhile, the above Surface1 and Surface2 are chosen as the analyzed objects to obtain the velocity distribution and streamline change characteristics to grasp the flow characteristics of the outer watershed of the photovoltaic inclined plate under different wind velocities.

The velocity distribution of Surface1 at different wind velocities is shown in Fig. 11. Overall, the outflow field of the photovoltaic inclined plate is clearly divided into zones at different wind velocities: the displacement zone before the airflow comes into contact with the photovoltaic inclined plate; the separation zone when the airflow flows through the photovoltaic inclined plate; and the cavity zone formed by the airflow on the backside of the photovoltaic inclined plate. Under different wind velocities, cavity areas are formed on the backside of the inclined plate and the support columns. Especially the backside of the photovoltaic inclined plate, which forms a cavity area that is much larger than the cavity area of the backside of the support column. Also compared the cavity area on the backside of the inclined plate at each wind velocity, it is found that the strength at high wind velocity is much higher than that at low wind velocity. At the inlet wind velocity $v=20\text{m/s}$, the center wind velocity in the cavity area is about 12.5m/s , with a large wind velocity difference from the cavity edge. While at the inlet wind velocity $v=5\text{m/s}$, the center wind velocity in the cavity area is about 5.0m/s , and the wind velocity difference with the cavity edge is small. It can be seen that the intensity of the vortex in the cavity region increases as the wind velocity increases. However, the change in inlet wind velocity has a small effect on the size of the cavity area, which is close to the influence area of the cavity at each wind velocity. It is also found that as the inlet wind velocity increases, the area and strength of the cavity area formed at the lower end of the inclined plate front increases. At $v=5\text{m/s}$, only a small cavity area exists at the lower end of the inclined plate front, and its velocity difference is small. And as the wind velocity increases, the cavity area increases significantly in size and intensity.

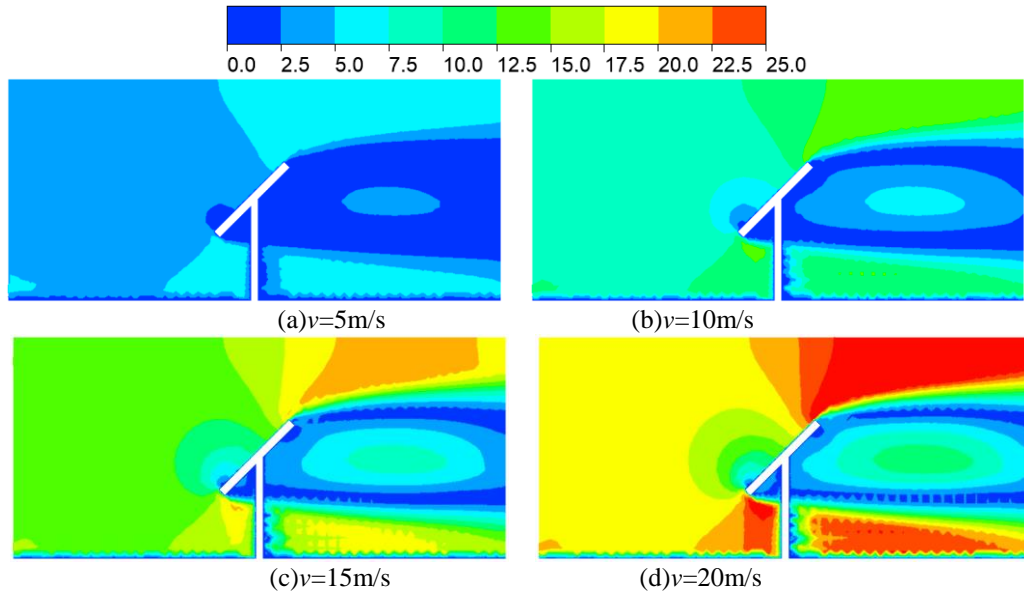


Fig. 11 Velocity distribution of Surface1 at different wind velocities (m/s)

The streamline diagram of Surface1 at different wind velocities is shown in Fig. 12. At this inclination angle, two distinct vortices are generated on the backside of the inclined plate, and the vortex zone is extremely coincident with the cavity zone at all wind velocities. It is also found that the streamlines are denser and stronger in the vortex zone at high wind velocities relative to the low wind velocities. However, the vortex zones at the same inclination angle are close to each wind velocity.

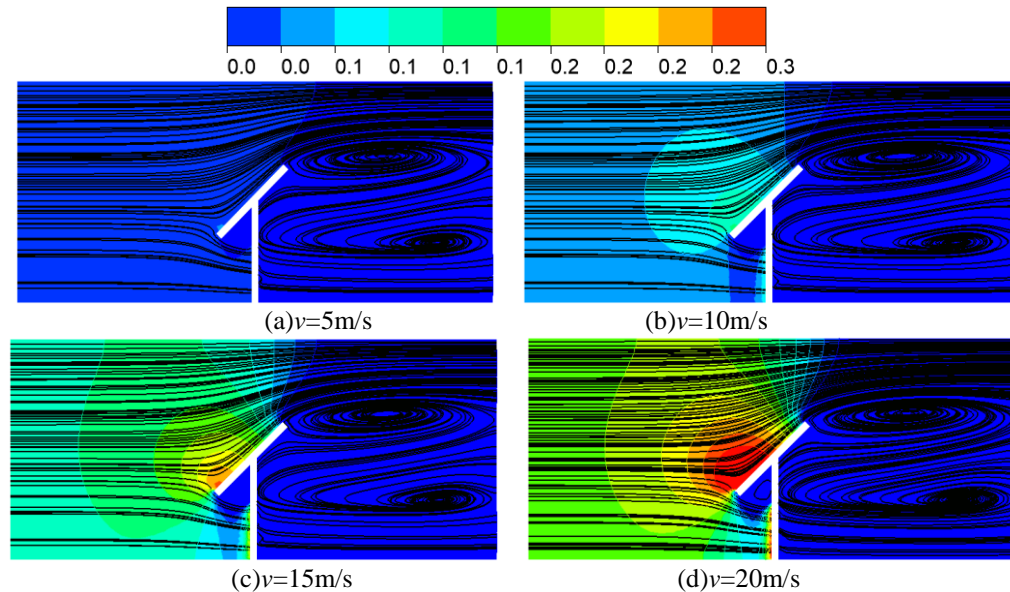


Fig. 12 Streamlines of Surface1 at different wind velocities (kPa)

The streamline diagram of Surface2 at different wind velocities is shown in Figure 13. Relative to Surface 1, the vortex area on Surface 2 is closer to the back of the inclined plate. For comparison, it is found that the streamlines in the vortex region are also denser and more intensive under high wind velocity inlet conditions. However, the vortex regions at all wind velocities remain close to each other.

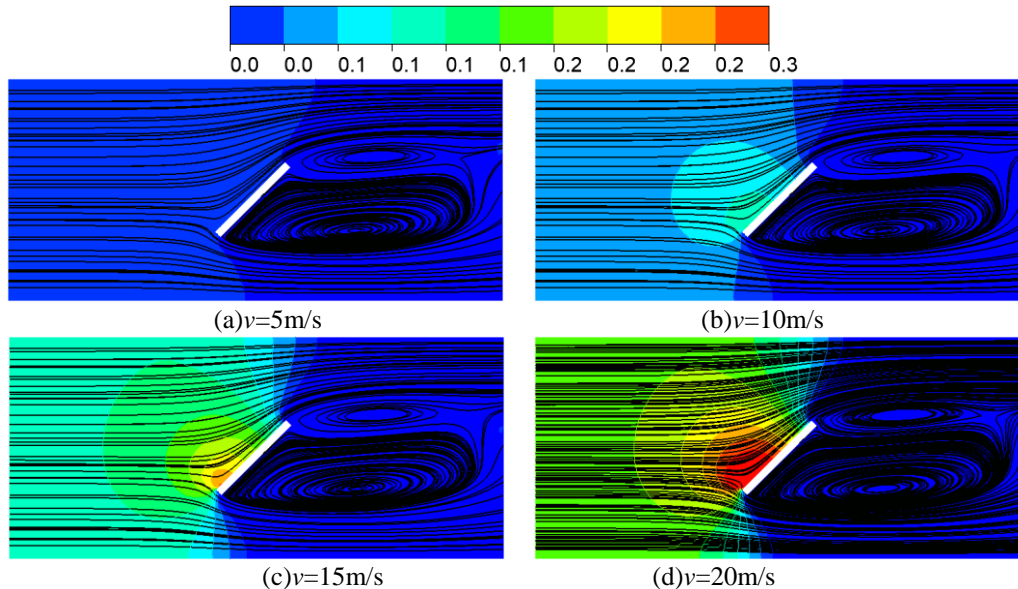


Fig. 13 Streamlines of Surface2 at different wind velocities (kPa)

IV. Conclusion

- (1) Under all flow conditions, the cavity area is formed at the back of the inclined plate, causing vortices. As the inclination angle of the inclined plate increases, the cavity area is larger and the streamlines at the vortex are denser and more intensive. As the inlet wind velocity increases, the streamlines at the vortex become denser and more intensive. However, the wind velocity has less effect on the size of cavity region and vortex region.
- (2) As the inclination angle of the photovoltaic inclined plate increases, the wind area is larger and the drag coefficient is greater.

Reference

- [1]. Implementation Program of Photovoltaic Power Generation Construction in 2015 [J]. Energy Saving of Nonferrous Metallurgy, 2015, 31(04): 3+2.
- [2]. Miller R D, Zimmerman D K. Wind loads on flat plate photovoltaic array fields. Phase III, final report[R]. Boeing Engineering and Construction Co., Seattle, WA (USA), 1981.
- [3]. He GL, Jiang HQ, Shan JD, et al. Research of Wind Load Model in Photovoltaic Array [J]. Electric Power Construction, 2012, 33(10): 5-8.
- [4]. Jiang JB, Zhang ZY, Lu YM, et al. Numerical analysis of wind loads about photovoltaic arrays considering bending moment [J]. Renewable Energy Resources, 2019, 37(01): 46-52.
- [5]. Gong M, Ou TY. Research on Wind Tunnel Test of Shape Coefficient of Wind Load for Photovoltaic Module with Single Roof [J]. ANHUI AEROSPACE, 2015, 22(06): 183-184.
- [6]. Hu RH, Xie C, Qin LP, et al. Calculation and Improvement for One Photovoltaic System [J]. Development & Innovation of Machinery & Electrical Products, 2010, 23(06): 20-22.
- [7]. Abiola-Ogedengbe A, Hangan H, Siddiqui K. Experimental investigation of wind effects on a standalone photovoltaic (PV) module[J]. Renewable Energy, 2015, 78: 657-665.
- [8]. Wei BC, Zhang GP, Miao GW, et al. Analysis of mechanical properties of fixed photovoltaic mounts during bearing settlement [J]. SOLAR ENERGY, 2019(03): 49-53.
- [9]. PFAHL A, COVENTRY J, ROGER M, et al. Progress in heliostat development[J]. Solar energy, 2017, 152: 3-37.
- [10]. Xiong Q, Li Z, Luo H, et al. Study of probability characteristics and peak value of heliostat support column base shear[J]. Renewable energy, 2021, 168: 1058-1072.

Shui-Sheng Xu. "Calculation of turbulence flow field around photovoltaic inclined plate based on CFD". *International Journal of Engineering Science Invention (IJESI)*, Vol. 12(10), 2023, PP 33-41.
Journal DOI- 10.35629/6734